Influence of Nozzle Parameters on Spray Pattern and Droplet Characteristics for a Two-Fluid Nozzle

Kathrin Kramm[1,*,‡], Maike Orth[1,*,‡], Arne Teiwes[1,2], Jana Christina Kammerhofer[3], Vincent Meunier[4], Swantje Pietsch-Braune[1], and Stefan Heinrich[1]

DOI: 10.1002/cite.202200152

Supporting Information available online

Dedicated to Prof. Dr.-Ing. Joachim Werther on the occasion of his 80th birthday

In this study, a two-fluid nozzle, as, e.g., used in fluidized-bed or spray drying applications, is comprehensively characterized regarding the spray pattern and droplet size. To analyze the spray cone, the spray cone angle and the radial mass distribution of the nozzle were measured at varied liquid flow rate, spray air pressure, liquid insert bore diameter, and air cap position. Additionally, droplet size distributions were recorded at different spray settings. In general, the overall spray cone and single droplets are significantly influenced by the spray parameters, especially the spray air pressure, as well as the nozzle geometry.

Keywords: Atomization, Droplet sizes, Spray angles, Spray patterns, Two-fluid nozzles

Received: July 30, 2022; *revised:* November 15, 2022; *accepted:* December 01, 2022

1 Introduction

1.1 Spraying of Liquids

The atomization and spraying of liquids are an essential operation in various industrial processes as well as in everyday life. The applications are wide-ranging and include, e.g., evaporative cooling, agriculture, firefighting, spray drying, and fluidized-bed processes [1, 2]. Liquid atomization is used to generate an increased surface area by comminuting the droplet diameter to obtain enhanced heat and mass transfer or chemical reactions [2, 3]. The droplet size distribution is thereby highly dependent on the nozzle type and design [1, 4–7]. In fluidized-bed operations, the nozzle configuration is one of the critical process parameters since depending on the selected settings, product quality can deteriorate and material may be lost [2]. To control the fluidized-bed granulation process, knowledge of the droplet size distribution, spray pattern, spray angle, and radial mass distribution of the spray is necessary as these markedly influence the particle-droplet interaction and thus the final particle size and morphology. Fluidized-bed processes with liquid injection for particle formulation applications often use two-fluid nozzles because a very fine droplet size spectrum is provided and a relatively large bore diameter of the liquid insert reduces the clogging potential of the nozzle. The design of the two-fluid nozzle consists of a centrally positioned liquid tube and a surrounding annular channel supplied with pressurized gas. For two-fluid nozzles, usually, high gas velocities are applied to enable the formation of a spray by atomization of low liquid volume flows [8]. Depending on the contact area of gas and liquid, a distinction is made between nozzles of internal or external mixing [9]. The internal mixing nozzle injects the liquid jet into the gas volume flow, while in the external mixing nozzle, the

[1]Kathrin Kramm,
Maike Orth https://orcid.org/0000-0002-0220-7705,
Arne Teiwes, Dr.-Ing. Swantje Pietsch-Braune, Prof. Dr.-Ing. habil. Dr. h.c. Stefan Heinrich
(kathrin.kramm@tuhh.de, maike.orth@tuhh.de)
Hamburg University of Technology, Institute of Solids Process Engineering and Particle Technology, Denickestraße 15, 21073 Hamburg, Germany.

[2]Arne Teiwes
Glatt Ingenieurtechnik GmbH, Nordstraße 12, 99427 Weimar, Germany.

[3]Dr.-Ing. Jana Christina Kammerhofer
Nestlé Product Technology Center, Nestléstraße 3, 3510 Konolfingen, Switzerland.

[4]Dr.-Ing. Vincent Meunier
Nestlé Research, Vers-Chez-Les-Blanc, Route du Jorat, 1005 Lausanne, Switzerland.

[‡]Both authors contributed equally to this paper.

contact between both phases happens at the nozzle outlet. For atomization of coating liquids or binders in the fluidized bed, two-fluid nozzles with external mixing are preferably used since clogging of the nozzle is less frequent due to the extended liquid input and the droplet diameter can be varied independently of the liquid volume flow. However, if the atomizer is used in the bottom-spray process, granule abrasion may occur near the nozzle orifice due to the high gas velocities [2].

The mechanism of droplet formation from a liquid jet is based on shear stresses due to high gas velocities. The turbulent fluctuations induce dynamic pressure forces that, upon overcoming the surface tension forces, lead to the breakup of the liquid into droplets [3]. In most cases, the liquid flow has low velocities compared to the gas, thus, fluid momentum is not considered. During the first phase, the liquid to be sprayed is broken up into filaments as well as larger droplets by the applied forces. In the second atomization phase, the diameter of those droplets is reduced [2]. Atomization effectiveness depends besides the nozzle geometry on the properties and the mass flows of both phases as well as the gas-to-liquid ratio. In case of air as atomizing gas, the latter is referred to as the air-to-liquid ratio (ALR) [3]. For low mass flow ratios between the gas and the liquid, the liquid jet is captured by the pressurized gas at a defined distance from the nozzle outlet and droplets are formed. With increasing mass flow ratios, a backflow of the liquid droplets and the gas phase is generated, leading to the formation of a fine droplet size spectrum [8].

1.2 Previous Works

The influence of the specific nozzle geometry and settings on the droplet size distribution and the relation to the spray angle has been investigated in several previous works. Mulhelm et al. [3] cite the gas velocity in relation to liquid flow rate being the largest influencing parameter on the mean droplet diameter. The atomization effectiveness can be increased by higher velocity differences between liquid and gas [2, 6]. Nyuttens et al. [10] describe a correlation between droplet size and velocity spectra as well as the relation of decreased droplet size distribution with increasing spray pressure. A narrower distribution function with increased air pressure is also postulated by Rizk et al. [11]. Juslin et al. [12] showed in studies using the pneumatic nozzle Model 940–943 of the company Schlick (Düsen-Schlick GmbH, Germany) that an increase in liquid flow rate did not have a significant effect on the droplet distribution pattern as well as the spray angle. But the liquid flow rate had an effect on the width of the droplet size distribution. A higher liquid volume flow resulted in an increase in the mean droplet diameter [1, 13]. The liquid velocity depends on the nozzle characteristics as well as spray liquid properties and feed pressure [9]. The gas pressure was identified as the primary factor influencing the spray angle since the dynamic force increases to a certain extent with increasing pressure [12]. Schick cites an inverse relationship between droplet size and spray angle, meaning that an increase of spray angle results in smaller droplet diameters [1]. Depending on the nozzle, a large spray angle can reduce the spray efficiency of the atomizer [9].

Vesvey et al. [13] determined the highest droplet velocity for the Schlick 970 two-fluid nozzle in the center of the spray, and the lowest velocities were measured at the edge of the spray area. Increased liquid viscosity and surface tension negatively affect the breakup mechanism, resulting in larger mean droplet diameters and a lower spray angle [3, 5, 13]. In contrast, Juslin et al. [12] reported that with increasing viscosity no clear influence on the droplet size distribution could be detected. High liquid density at constant nozzle parameters results in a more compact spray that is less affected by the atomization gas [2]. In literature, different droplet size correlations for nozzles with external mixing are present based on various fluid properties as well as methods of droplet size measurement [3, 11, 14–17]. However, the influence of the parameters on the resulting droplet size as well as spray angle is strongly dependent on the design and size of the nozzle [10]. Thus, in fluidized-bed processes, it is particularly necessary to know the influencing factors for a specific nozzle more precisely and to characterize them in advance to achieve defined spray and product properties. Therefore, a novel well reproducible, step-wise measurement and data analysis procedure for spray characterization is proposed.

2 Applied Methods

As influencing spray parameters, the liquid spray rate, the spray air pressure, the bore diameter of the liquid insert, and the air cap position were varied to analyze their effect on the spray. For all experiments, water was used as spraying liquid and the liquid was atomized with compressed air.

2.1 Radial Mass Distribution of the Nozzle Spray

The nozzle spray was characterized according to the radial mass distribution using a setup of ten cylindrical shells with a diameter between 2 and 20 cm. The diameter of the individual shells was varied by 2 cm in ascending order with a wall thickness of 1 mm. The shells were made of polylactide and produced in a 3D printer (Ultimaker, Netherlands). For the measurement, the individual shells were inserted into each other. To prevent slipping, additional rings were printed that allow a flush plugging together. The two-fluid nozzle 970 S4 (Düsen-Schlick GmbH, Germany) was placed at a varied distance d from the shells of 10 cm, 15 cm, or 20 cm as shown in Fig. 1.

The influence of different parameters on the radial mass distribution of the nozzle was investigated by varying the

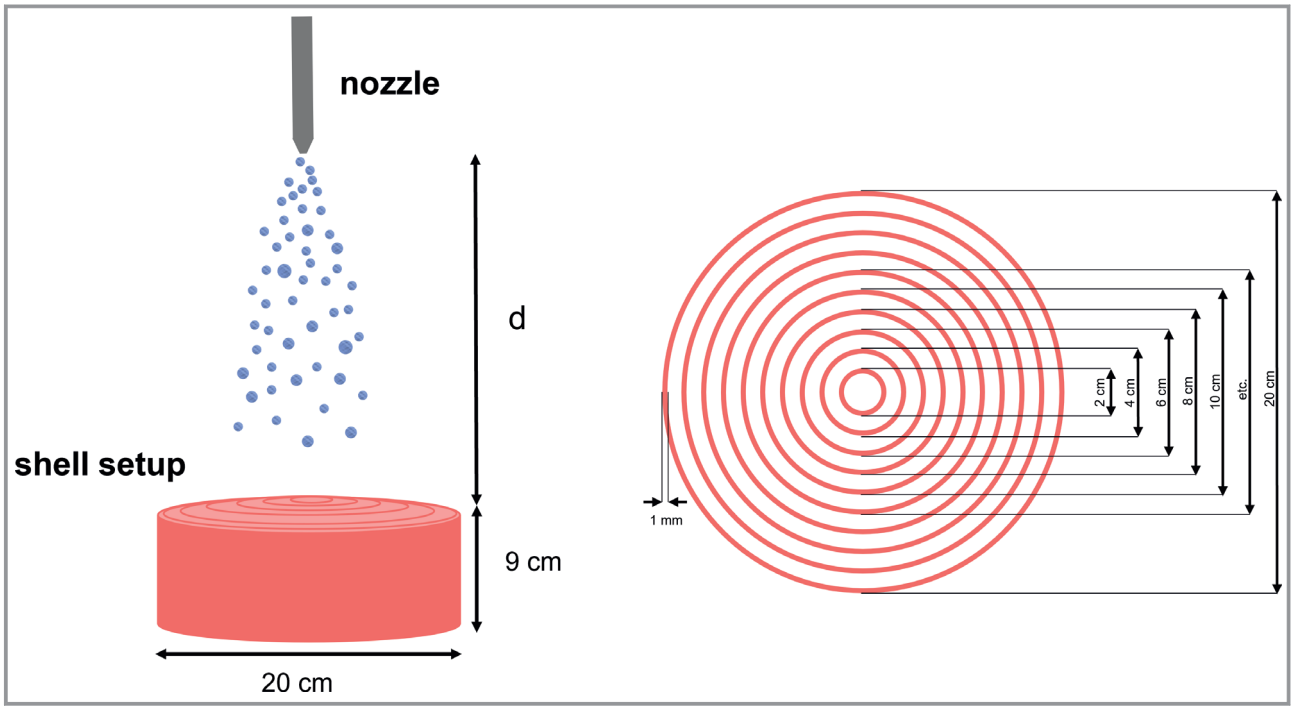

Figure 1. Scheme of the spray patternator setup for the spray mass distribution measurements.

liquid spray rate between 5 g min^{-1} and 30 g min^{-1} at air pressures of 0.5 bar, 1.5 bar, and 2.5 bar. These settings would, e.g., be suitable for fluidized-bed or spray drying experiments on a laboratory scale. The air cap position of the nozzle was adjusted with one as well as two full turns which resulted in a varied distance between the air and liquid outlet (see Fig. 2). Additionally, the experiments were conducted using liquid inserts with bore diameter of 1.0 mm and 1.2 mm. The water was conveyed to the nozzle with a peristaltic pump (Medorex TB, Germany). For each run, the spraying process was carried out until one cylinder was completely filled with water or for a maximum of 11 min at lower spraying rates. The previously balanced shells were weighed individually and the percentage by mass of the water contained was calculated.

2.2 Spray Cone Angle

As shown in Fig. 2, the experimental setup for spray cone angle measurement consisted of a light source, a high-speed camera NX-S2 (Imaging Solutions GmbH, Germany), and the two-fluid nozzle of type 970 S4. For the spray rate, air pressure, and diameter of the liquid insert, the same values as in Sect. 2.1 were applied. The air cap position of the nozzle was also changed between positions 0 and 6, where position 0 indicates a full cap turn and the remaining positions were set according to the number of the air cap.

The images of the nozzle spray generated with the experimental setup were analyzed using the software MATLAB

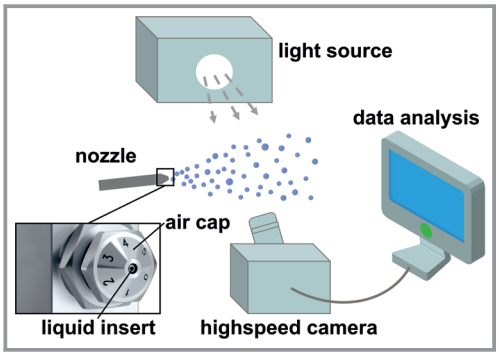

Figure 2. Scheme of the spray cone analysis setup [18].

(the MathWorks, Inc., USA). Only images in which the spray jet is clearly visible were selected. First, the original image was cut in such a way that only the spray cone in front of a dark background is visible. This image was then converted into a grayscale image from which a histogram over the different gray levels was generated ranging from 0 (white) to 255 (black). A threshold was chosen based on the peak in this histogram and applied consistently to all images of the spray jet to obtain a binary image consisting of a white spray cone area and a black background. By performing image opening on the binary image, black pixels that might be present within the spray cone area were changed to white, so a continuous white area without black holes was guaranteed. Afterwards, the borders of the spray area were detected in each column of the image. From this data, the outlines of the spray

cone were approximated by a linear function from which the spray cone angle was calculated.

2.3 Droplet Size Distribution

The nozzle spray droplet size distribution was measured by means of laser diffraction with the Malvern Panalytical Spraytec system (Malvern Panalytical GmbH, Germany). Therefore, the Malvern Panalytical Spraytec system was integrated in a spray measurement booth as displayed in Fig. 3. The droplet size distribution data was obtained by measuring the intensity of light scattered as a laser beam passes through a spray at a distance of 100 mm from the nozzle tip. This data was then analyzed to calculate the volume-based size distribution of the droplets that created the scattering pattern. The measurement range of the system was 0.1–2000 µm with a measurement rate of up to 10 000 measurements per second.

Analogously to Sects. 2.1 and 2.2, the influencing parameters were examined by varying the liquid spray rate, air pressure, and bore diameter of the liquid insert. The air cap position of the nozzle was considered to be the standard cap position 4. For each measurement, the following procedure was applied: the spray liquid (water, 20 °C) was prepared in sufficient amount and the liquid spray rate was calibrated by gauging the correctly configured liquid spray pump. After proper connection of all feedlines to the nozzle, the measuring booth was darkened and booth aeration was started. After completion of the background zero measurement, spray was started and measured for at least 60 s.

3 Results and Discussion

3.1 Radial Mass Distribution

The radial mass distribution of the nozzle was investigated to deduce, e.g., in which area of the spray zone the most particles are wetted in a fluidized bed. Parameter variations are also used to examine the impact on the distribution. In Fig. 4a, the influence of different atomization pressures for the liquid insert of 1.2 mm, distance between the nozzle and boxes of 10 cm, and liquid spray rate of 20 g min^{-1} is shown. For the highest spray air pressure, the largest percentage of water is in the boxes with the diameter of 6 cm and 8 cm. The higher air pressure of the nozzle results in a higher maximum water amount in the inner shells, the lowest pressure of 0.5 bar is characterized by higher mass fractions of the spray liquid in the area of large shell diameters. Fig. 4b (liquid insert of 1.0 mm) illustrates that an increase in the atomization pressure causes decreasing spray angles and, thus, more water is collected in the inner shells. The largest amount of water was found in the second and third shells from the center. In particular, the percentage water fraction increases with increasing air pressure. The dependence on the measurement distance is summarized for one parameter setting in Fig. 5. As the distance between the nozzle orifice and the shells increases, a broader radial mass distribution is obtained which gets narrower with increasing atomization pressure and is concentrated on the centrally placed shells. Furthermore, the radial mass distribution measured at different nozzle-to-shell distances characterizes the overall shape of the spray cone and serves as an indicator for the spray angle. The broader distribution at higher distance shows the increasing spray radius upon progressing further from the nozzle tip and, thus, the cone-like shape of the spray. By defining a percentage of water mass that is representative of the overall spray cone and evaluating the diameter at which that mass is included, the edge of the spray could be determined. From that, the spray angle could be calculated. However, since only three points along that edge are known at each parameter combination, the radial mass was not used for quantification of the spray angle. Instead, the image-based measurement as described in Sect. 2.2 was chosen to obtain more refined data.

In Fig. 6a, two different air cap positions have been used with the liquid inserts of 1.0 mm and 1.2 mm at 10 cm distance. For both fluid inserts, cap position 6 results in a larger radial mass distribution compared to cap position 0.

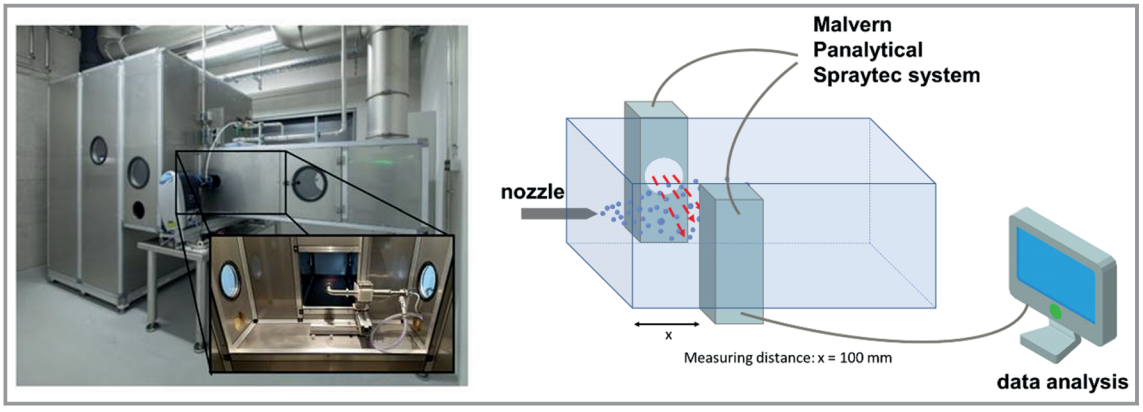

Figure 3. Measurement setup for the determination of droplet size distribution using laser diffraction from Malvern Panalytical Spraytec system.

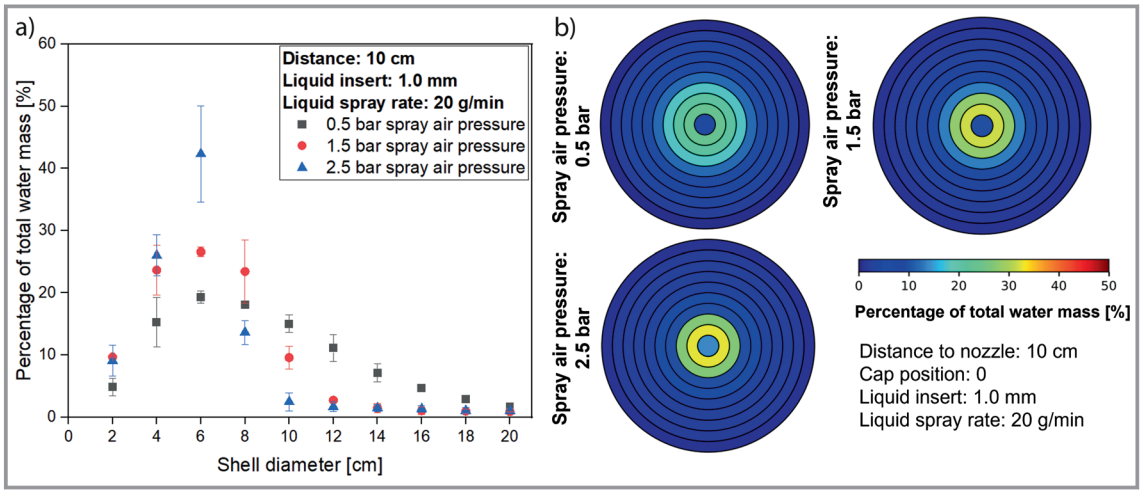

Figure 4. a) Percentage of total water mass as a function of shell diameter at a distance of 10 cm, liquid insert of 1.2 mm, cap position 0, liquid spray rate of 20 g min^{-1} for atomization pressures of 0.5 bar, 1.5 bar, and 2.5 bar; b) graphical representation of the spray pattern in the shells at different spray air pressures with otherwise constant parameters for the liquid insert of 1.2 mm.

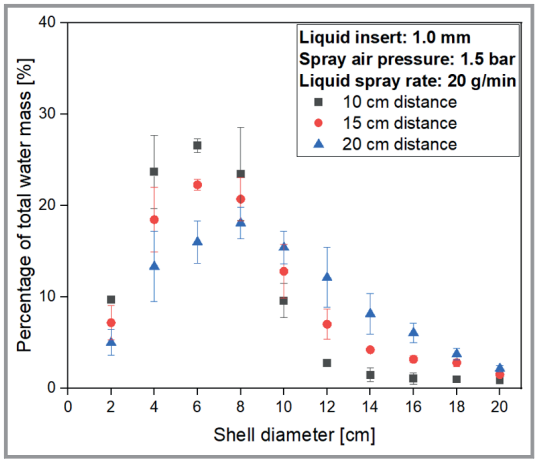

Figure 5. Percentage of total water mass as a function of shell diameter for the distances 10 cm, 15 cm, and 20 cm at constant parameters of 1.0 mm liquid insert, air cap position 0, 20 g min^{-1} liquid spray rate, and 1.5 bar spray air pressure.

For cap position 0, the velocity of compressed air in the two-fluid nozzle at the contact point with the liquid is assumed to be higher. This consequently leads to a more centric distribution. Since the use of the 1.2 mm wide liquid tube reduces the annular gap to the air cap, the gas velocity is higher compared to the 1.0 mm liquid insert. This is manifested in the generated data by a significantly higher maximum value for the shell diameter of 6 cm, whereas the remaining shells show lower percentage liquid amounts. For the trials with the distances of 15 cm and 20 cm (not shown here), the shell diameters of 4 cm to 10 cm contained larger percent water amounts at air cap position 6 compared to position 0. The different trend between the distances can probably be attributed to non-collected water in the boxes since at higher distances the risk of the spray cone width exceeding the largest box diameter is increased.

Fig. 6b illustrates an example of the radial mass distribution for the liquid insert of 1.0 mm, atomization pressure of 1.5 bar at a distance of 10 cm between the shells and the nozzle orifice for different liquid spray rates. Further diagrams can be found in the Supporting Information. The graph indicates that the spray rate has an influence on mass distribution. An increase in liquid spray rate is expressed in the centric distribution, where the peak of the distribution is shifted from the box with diameter 4 cm toward the 6 cm box. The change in the distance between the nozzle orifice and the trays is also reflected here with an accumulation of water in the outer shells as the liquid flow rate changes. The alteration in the liquid insert is evident in the radial mass distribution of the nozzle spray. The usage of the 1.2 mm fluid insert provides higher percentages of water mass for the inner shells.

3.2 Spray Cone Angle

Fig. 7 shows the spray angle in dependence on the ALR for varied spray air pressures and liquid inserts. In the following section, the influence of these different parameters in the spray angle is discussed in detail.

3.2.1 Air-to-Liquid Ratio

In general, the spray cone angle decreases with increasing ALR, as shown in Fig. 7. These observations confirm the findings of Lefebvre [19]. Higher values of ALR indicate either a lower liquid spray rate or higher spray air flow while keeping the other parameters constant, respectively. The highest spray angles were observed at the lowest ALR of 1.3 meaning that at this value, the spray was spread the widest in radial direction at a given distance from the nozzle tip. By increasing the liquid spray rate, the velocity of the

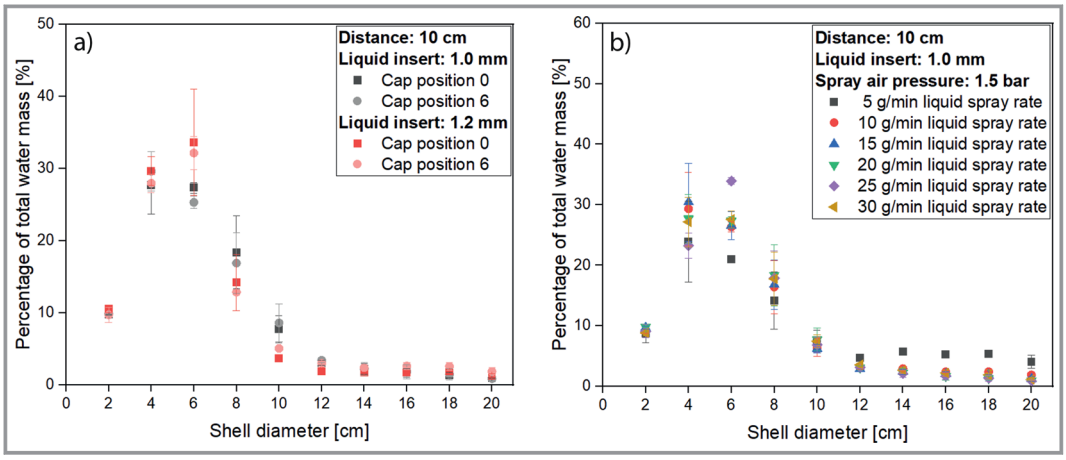

Figure 6. Percentage of total water as a function of shell diameter at a distance of 10 cm and spray air pressure of 1.5 bar. a) Liquid spray rate of 20 g min^{-1} with liquid inserts of 1.0 mm and 1.2 mm with varying cap position, b) with liquid insert of 1.0 mm at cap position 0 and varying liquid spray rates.

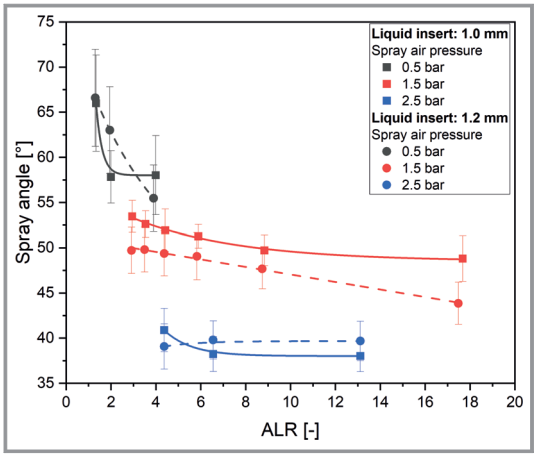

Figure 7. Spray cone angle as a function of air-to-liquid ratio (ALR) at different spray air pressures of 0.5 bar, 1.5 bar, and 2.5 bar for the liquid inserts 1.0 mm and 1.2 mm.

liquid is also increased which reduces the ALR as well as the relative velocity between air and water and, thus, the frictional force on the liquid surface. Furthermore, Lefebvre [19] describes that the relative velocities between the spray air and liquid have an additional effect beyond the velocities of the two fluids. As described by Hede et al. [2], the air cannot penetrate the liquid jet at higher liquid velocities resulting in higher spray angles. Low velocity liquid jets, however, can easily be penetrated by the high velocity air, thus, a spray cone with narrow angle is formed due to the high turbulences and energy transfer. This increased turbulence can quantitatively be seen in the Reynolds number of the air. While at all investigated air pressures the air flow is turbulent, the Reynolds number at 2.5 bar is more than three times higher than at 0.5 bar, which translates to significantly higher inertia forces. This influences both primary and secondary droplet breakage creating different spray patterns and droplet sizes. For two-fluid nozzles with external mixing, as the one used in this study, the increase of ALR additionally leads to a backflow of air and droplets [8].

If the spray air pressure and, thus, the air velocity is increased, more energy is introduced into the system shaping the liquid jet in such a way that a narrow spray cone with a smaller angle is formed. Liu et al. [6] also measured a contraction of the spray cone at increased spray pressure due to the pronounced momentum exchange. In contrast, at lower spray air pressures and therefore lower ALR, the relative velocity between air and liquid is smaller resulting in a wider spray pattern with higher cone angle. These findings are in accordance with the radial mass distributions discussed in Sect. 3.1, where at low spray air pressure and lower ALR, more water was detected in the outer shells than for higher pressure.

Comparing the curves at different pressures, a different degree of impact of the ALR on the spray angle becomes apparent. At the lowest spray air pressure of 0.5 bar, a decrease from 66.0 ± 5.3° to 58.0 ± 4.4° was observed when increasing the ALR from 1.3 to 4.0 with the 1.0 mm liquid insert. However, at 2.5 bar, an increase in ALR by 8.7 only resulted in a spray angle decrease of from 40.9 ± 2.4° to 38.0 ± 1.7°. This reduced influence of the ALR at higher pressures is related to the changed flow behavior of the air at different velocities. When increasing the spray air pressure form 0.5 bar to 2.5 bar, the pressure regime changes which induces a varied structure of gas flow in addition to the effect of the ALR.

3.2.2 Nozzle Setup

In addition to the water and air flow, the setup of the nozzle has been varied to investigate the influence on the spray cone angle. Therefore, the bore diameter of the liquid inserts as well as the air cap position were changed for the spray experiments respectively. Comparing both diagrams

in Fig. 7, slightly lower spray angles can be observed for the larger opening of 1.2 mm and otherwise the same parameters. Due to the increased area for the water and at the same time smaller area for the air, the relative velocity between both phases increases since the liquid velocity decreases while the gas velocity increases. Thus, a narrower spray cone results from a larger liquid insert bore diameter.

Fig. 8 shows the spray angle in dependence on the air cap position at a liquid flow rate of 20 g min^{-1} and spray air pressure of 1.5 bar. For the liquid insert with a bore diameter of 1.2 mm and air cap positions from 1 to 5, larger spray angles were measured at increased distances between the liquid and air outlet. Varying the air cap position results in a changed velocity when the liquid encounters the gas and thus influences the breakup mechanism. At higher cap positions and therefore larger distance between gas and liquid outlet, a reduced relative velocity between air and the spraying liquid water at the contact point of both phases is expected. If the liquid outlet is the furthest away from the air outlet (position 6), the air velocity is the lowest when coming into contact with the liquid, thus creating a wide spray cone. However, no clear trend is visible in the data recorded for the 1.0 mm liquid insert, where the highest spray angle was measured at cap position 1 and the lowest angle at position 5. Overall, the effect of the cap position on the cone angle seems to be less pronounced compared to the other influences discussed in this paper.

The spray angle at cap position 0 in particular is characterized by high variance for both bore diameters. At this position, the liquid outlet and the gas outlet are aligned which results in the air flow directly colliding with the water jet at the end of the conically shaped air cap. At the other positions in contrast, the air first collides with the tip of the liquid insert which directs the air stream in a parallel direction to the water jet creating a more structured flow pattern. The high air velocity in a co-current flow with the liquid then causes a narrower spray cone compared to cap position 0, where the deflection of the gas by the liquid insert does not occur.

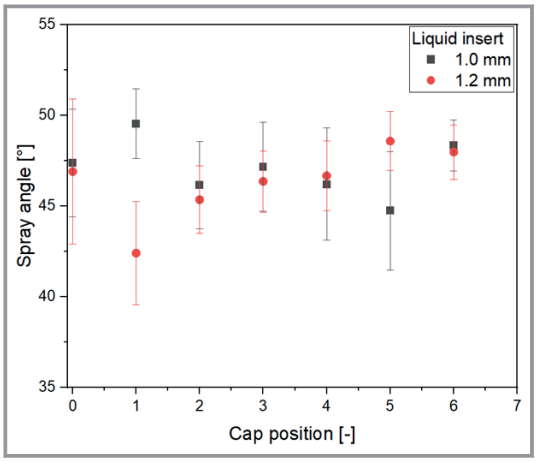

Figure 8. Spray cone angle as a function of air cap position for the liquid inserts of 1.0 mm and 1.2 mm at a liquid spray rate of 20 g min^{-1} and spray air pressure of 1.5 bar.

3.3 Droplet Size

Exemplarily, two droplet size distributions are shown in Fig. 9 at different liquid spray rates and variation of the spray air pressure for a liquid insert with 1.2 mm bore diameter. As is sufficiently known, the droplet sizes created by the nozzle decrease with increasing spray air pressure due to dynamic pressure forces and shear stresses during atomization resulting in a more effective droplet comminution [3]. This can be seen from the droplet size distribution shifted to the left for exemplarily shown spray rates.

Rizk and Lefebvre [11] also found a lower number of larger droplets in the spray with increasing gas velocity. Richter [8] explains the finding with the mass flow ratio between gas and liquid. An increase in the differential velocity between the two fluids results in finer spray due to an increase in the axial and tangential velocity of the particles and backflow of the droplets and gas [6, 8].

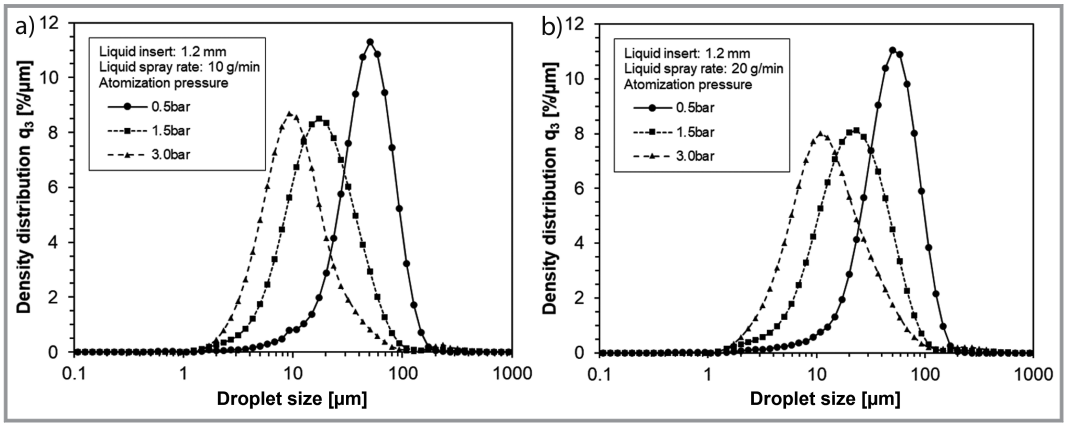

Figure 9. Density distribution of the droplet diameter for the liquid insert of 1.2 mm and at varying spray air pressures of 0.5 bar, 1.5 bar, and 3.0 bar at a liquid spray rate of a) 10 g min^{-1} and b) 20 g min^{-1}.

For the diagrams in Fig. 9, characteristic values of the volume-based droplet size distribution are shown in Tab. 1. As can be seen from the table, an increase of spray rate and spray air pressure also increases the SPAN values of the droplet size distributions compared to lower spray rates and spray air pressures. The SPAN value indicates the distribution width of the droplet size measurement, which describes a large distribution width with increasing value. The SPAN value is calculated from the difference between $x_{90,3}$ and $x_{10,3}$ to the quotient of $x_{50,3}$. Furthermore, droplet sizes increase slightly for higher spray rates at otherwise constant spray parameters. Similar to the spray angle, the most significant change in droplet size is observed when comparing the values at 0.5 bar and 1.5 bar due to the different gas flow regimes. The biggest increase can be observed for the $x_{90,3}$ values at higher spray rates at constant spray air pressure. The investigations are consistent with the findings in literature [3, 6, 11, 13].

4 Conclusions

An extensive characterization of the spray generated by the two-fluid nozzle Schlick 970 S4 was conducted to obtain a better understanding of how spray parameters and nozzle setup influence the single droplets as well as the overall spray cone. Therefore, the radial spray mass distribution, the spray cone angle, and the droplet size distribution were measured at varied nozzle settings. Among the investigated parameters, the spray air pressure was identified as primary influence on the spray angle and the mass distribution as well as the droplet size distribution. In general, narrow spray cones consisting of small liquid droplets were formed at high relative velocities between the gas and liquid phase due to the high shear forces acting on the liquid. These high velocities occurred at high spray air pressures, low liquid spray rates, large liquid insert bore diameters, and a short distance between the air and water outlet which all contribute to either a high gas or low liquid velocity at the contact point of both phases.

Future studies will be concerned with the investigation of material properties like dynamic viscosity and surface tension of the liquid phase on the atomization as well as the transfer of the findings to fluidized-bed applications like coating and agglomeration experiments. With a deeper understanding of the liquid injection, the spray in these applications can then be adjusted to create optimal process conditions to achieve desired product properties. If, e.g., a coating with a smooth surface should be formed, small liquid droplets should be sprayed onto the particles, which then can form a uniform coating layer without any significant surface defects [20]. For a process, where strong agglomeration is desired, lower spray air pressures and higher liquid flow rates should be chosen to achieve a high droplet size that enables the formation of stable liquid bridges. Depending on the size of the fluidized bed, the spray angle can be set to minimize wall spraying while still forming a large spray zone to wet the fluidized particles. Furthermore, knowledge about the spray is valuable for scale-up of the process since the droplet size distribution should be comparable to the laboratory-scale to achieve the same product properties while the mass flow of the liquid is significantly increased. For these considerations, especially the spray air pressure and air-to-liquid ratio are of importance. Besides the use in experiments, information about spray pattern and droplet size is also of great value for the simulations of fluidized-bed processes with computational fluid dynamics and the discrete element method, where these data are needed to initialize the nozzles as, e.g., done by Kieckhefen et al. [21].

Supporting Information

Supporting Information for this article can be found under DOI: https://doi.org/10.1002/cite.202200152.

Table 1. Characteristic droplet size parameters for different spray air pressure and liquid spray rates at the liquid input of 1.2 mm.

Spray air pressure [bar]	Liquid spray rate [g min^{-1}]	$x_{10,3}$ [µm]	$x_{50,3}$ [µm]	$x_{90,3}$ [µm]	x_{32} [µm]	SPAN [–]
0.5	10	21.7	47.2	87.8	34.1	1.40
	20	22.6	48.2	91.6	35.1	1.43
1.5	10	7.2	18.2	41.5	13.2	1.88
	20	7.9	21.7	50.3	14.8	1.96
3.0	10	4.5	10.9	25.4	8.5	1.91
	20	4.9	13.4	34.9	9.6	2.24

K. Kramm is financially supported by Nestec Ltd. and would like to thank Nestlé Research and Development for the assistance. M. Orth acknowledges funding from the German Research Foundation within the DFG Graduate School GRK 2462 "Processes in natural and technical Particle-Fluid-Systems (PrintPFS)" (Project No. 390794421). The authors would like to thank Philipp Grohn for the useful comments during implementation and Sophia Rothberg for proofreading as well as Brigham Watson, Noreen Niemeyer, Sam Dors, and Christoph Wolter for the support with the measurements. The authors would also like to thank Jochen Thies and Chris Baer for provision of data and assistance with the droplet size measurements at the Glatt Innovation Center in Binzen, Germany. Open access funding enabled and organized by Projekt DEAL.

Symbols used

d	[cm]	distance between nozzle and shells
x	[µm]	droplet diameter

Sub- and superscripts

10,3	10 % of the total volume
32	Sauter
50,3	50 % of the total volume
90,3	90 % of the total volume

Abbreviation

ALR	air-to-liquid ratio

References

[1] *Spray Technology Guide: Understanding Drop Size* (Ed: R. J. Schick), Spray Analysis and Research Services, Wheaton, IL **2008**.
[2] P. D. Hede, P. Bach, A. D. Jensen, *Chem. Eng. Sci.* **2008**, *63 (14)*, 3821–3842. DOI: https://doi.org/10.1016/j.ces.2008.04.014
[3] B. Mulhem, G. Schulte, *Atomization Sprays* **2003**, *13 (2–3)*, 23. DOI: https://doi.org/10.1615/AtomizSpr.v13.i23.100
[4] I. Zytynski, *What's in a spray? The four basic spray patterns and the characteristics of spray*, Technical Note, The Spray Nozzle People, Lewes, UK **2021**. www.spray-nozzle.co.uk/docs/default-source/default-document-library/whats-in-a-spray.pdf
[5] *A Summary of Tank Mix and Nozzle Effects on Droplet Size*, Spray Drift Task Force, Macon, MO **2001**.
[6] X. Liu, R. Xue, Y. Ruan, L. Chen, X. Zhang, Y. Hou, *Cryogenics* **2017**, *83*, 57–63. DOI: https://doi.org/10.1016/j.cryogenics.2017.01.011
[7] L. Juslin, O. Antikainen, P. Merkku, J. Yliruusi, *Int. J. Pharm.* **1995**, *123 (2)*, 257–264. DOI: https://doi.org/10.1016/0378-5173(95)00082-T
[8] T. Richter, *Zerstäuben von Flüssigkeiten: Düsen und Zerstäuber in Theorie und Praxis*, Expert Verlag, Renningen, Germany **2017**.
[9] N. Ashgriz, *Handbook of Atomization and Sprays: Theory and Applications*, Springer, Boston, MA **2011**.
[10] D. Nuyttens, K. Baetens, M. de Schampheleire, B. Sonck, *Biosyst. Eng.* **2007**, *97*, 333–345.
[11] N. K. Rizk, A. H. Lefebvre, *J. Eng. Gas Turbines Power* **1984**, *106 (3)*, 634–638. DOI: https://doi.org/10.1115/1.3239617
[12] L. Juslin, O. Antikainen, P. Merkku, J. Yliruusi, *Int. J. Pharm.* **1995**, *123 (2)*, 247–256. DOI: https://doi.org/10.1016/0378-5173(95)00081-S
[13] C. Vesvey, J. Cronlein, A. Breuer, S. Gerstner, *Fluid Bed Nozzle Spray Characterization of an Aqueous Ethylcellulose Dispersion for Particle Taste-Masking Applications*, Colorcon, West Point, PA **2014**.
[14] J. Gretzinger, W. R. Marshall, *AIChE J.* **1961**, *7 (2)*, 312–318. DOI: https://doi.org/10.1002/aic.690070229
[15] P. Walzel, *Int. Chem. Eng.* **1993**, *33*, 1.
[16] B. Mulhem, G. Schulte, U. Fritsching, *Chem. Eng. Sci.* **2006**, *61 (8)*, 2582–2589. DOI: https://doi.org/10.1016/j.ces.2005.11.035
[17] D. A. Nguyen, M. J. Rhodes, *Powder Technol.* **1998**, *99 (3)*, 285–292. DOI: https://doi.org/10.1016/S0032-5910(98)00125-9
[18] www.myschlick.com/fileadmin/user_upload/Downloads/SCHLICK-Downloads/Catalogue-excerpts/de-gb/ca-two-substance-nozzles-model-970-de-gb.pdf (Accessed on July 29, 2022)
[19] A. H. Lefebvre, *Atomization and Sprays*, Hemisphere, New York **1989**.
[20] M. Orth, P. Kieckhefen, S. Pietsch, S. Heinrich, *KONA* **2022**, *39*, 230–239. DOI: https://doi.org/10.14356/kona.2022016
[21] P. Kieckhefen, S. Pietsch-Braune, S. Heinrich, *Processes* **2022**, *10 (7)*, 1291. DOI: https://doi.org/10.3390/pr10071291

